JOURNAL OF COMPUTATIONAL PHYSICS 112, 370–381 (1994)

A Variant of Van Leer's Method for Multidimensional Systems of Conservation Laws

BENOÎT PERTHAME

Laboratoire d'Analyse Numérique, Université Paris 6 et CNRS, T55/65 étage 5, 4 place Jussieu, 75252 Paris Cédex 05, France; and INRIA, Projet MENUSIN, B.P. 105, 78153 Le Chesnay Cédex, France

AND

YOUCHUN QIU

INRIA, Projet MENUSIN, B.P. 105, 78153 Le Chesnay Cedex, France

Received March 29, 1993

We present a new variant of Van Leer's construction of upwind finite volume schemes for hyperbolic systems of conservation laws. Fluxes are computed with second-order accuracy using an interpolation rather than a slope reconstruction. A correction of the interpolated values is necessary and performed globally on each cell by a conservation argument. It can be used on a rectangular or triangles based dual grid to obtain a genuinely multidimensional scheme. One of our main concerns in this construction, is to prove that the second-order reconstruction, combined with a Boltzmann solver, gives nonnegative values of the pressure and density for gas dynamics, even on an unstructured mesh. This allows us to derive a rigorous CFL condition. Thus our approach is very robust.

1. INTRODUCTION

In this paper, we present a new upwind finite volume scheme for solving multidimensional hyperbolic systems of conservation laws on unstructured grids. It is a variant of Van Leer's idea [18] which has been leading much of the recent research in this area, see, for instance, Collela [2], Durlofsky, Engquist, and Osher [6], Sanders and Wieser [15], and the references therein. Van Leer's method consists in introducing a limitation step in the calculation of the gradients necessary for a second-order accurate evaluation of the fluxes in the finite volume formulation. This limitation turns out to be necessary to avoid oscillations in the numerical results, as it is well understood for scalar conservation laws in 1D because of "TVD" properties (Harten [9]). But for multidimensional systems, the limitation of gradients is very unnatural and, for instance, direction by direction limitations are not satisfactory.

The main ideas we propose here are first to avoid the gradient constructions, just replacing them by an interpolation. This leads us to represent the solution, no longer as a piecewise linear function by cell, but by a piecewise constant on subcells function (p.c.s. function in short). This interpolation is natural when dealing with a rectangular mesh or a triangle-based dual mesh and this last case will be considered throughout this paper. Second, the limitation step is performed by a conservation argument on each cell for this p.c.s. function. It is global on the cell and does not require predetermined directions.

Another motivation for the precise construction we propose is gas dynamics equations. Then, we are able to prove that the computed densities and pressures remain nonnegative, which leads us to derive a rigorous CFL condition on the time step. This kind of nonlinear stability condition appears to be useful for several types of computations: interaction of strong shocks as in the blast waves problem, low density, and pressure zone behind a body in a hypersonic regime (see also the 1D test problems proposed by Einfeldt, Munz, Roe, and Sjögreen [7]), multicomponent reacting gases (see Fezoui and Larrouturou [8]), adaptive mesh technics which lead to very distorted triangles. This nonnegativity property requires us to use a basic upwinding algorithm that preserves nonnegativity at least for one-dimensional problems. Thus we choose to use the Boltzmann solver (Deshpande [4], Perthame [13], Pullin [14]) because it reduces the nonlinear gas dynamics equations to a linear kinetic equation, thus allowing a positivity analysis. The counterpart to the robustness of this solver, is that its flux splitting form makes it very dissipative on stationary contact discontinuities (slip lines along a body in particular). This is reported in Coquel and Liu [3], for instance.

For ease of presentation, we will now restrict ourselves to

0021-9991/94 $6.00

solving the gas dynamics equations on a dual grid. In Section I below we recall these equations, make more precise the construction of this grid, and introduce the main notations. Then, in Section II we present our interpolation algorithm, the limitation by conservation, and prove that it is second-order accurate. Finally, in Section III we show that, together with this algorithm, the kinetic solvers preserves the nonnegativity of density and pressure. Numerical results are presented in Section IV.

2. DESCRIPTION OF THE SCHEME ON AN UNSTRUCTURED GRID

In this section, we give a general presentation of the finite volume scheme and we leave for the next section the details of the interpolation and limitation algorithm. Note that it is a multidimensional extension of a 1D algorithm proposed in [13], where both second-order accuracy and nonnegativity of densities and pressures were obtained. For the sake of simplicity we restrict ourselves to the case of gas dynamics and to a single example of grid: the dual one in two dimensions.

2.1. Gas Dynamics and Dual Grid

We now consider the system of gas dynamics equations in two space dimensions

$$\partial_t U + \operatorname{div}_x F(U) = 0, \qquad x \in \mathbb{R}^2, \qquad t \geqslant 0, \tag{1}$$

where the unknowns $U(t, x)$ are given by

$$U = (\rho, \rho u_1, \rho u_2, E), \tag{2}$$

and the flux $F(U) = (F_1(U), F_2(U))$, with

$$\begin{aligned} F_1(U) &= (\rho u_1, \rho u_1^2 + p, \rho u_1 u_2, E u_1), \\ F_2(U) &= (\rho u_2, \rho u_1 u_2, \rho u_2^2 + p, E u_2), \end{aligned} \tag{3}$$

$$E = \tfrac{1}{2}\rho\,|u|^2 + \rho\varepsilon, \qquad p = \rho T = (\gamma - 1)\,\rho\varepsilon, \qquad 1 < \gamma \leqslant 2. \tag{4}$$

The construction of the numerical algorithm, the limitation procedure, and the accuracy analysis below can be applied to a large extent to general systems. But our nonnegativity analysis is restricted to gas dynamics and thus we prefer to deal directly with this system.

Next let us describe the grid we are going to use for our finite volume scheme. It has already been used in gas dynamics by Angrand, Dervieux, Boulard, Périaux, and Vijayasundaram [1], Rostand and Stoufflet [15]. The basis is a given triangulation with vertices positioned at points $(X_i)_{1 \leqslant i \leqslant I}$.

The cell C_i is the control volume delimited in joining the mass centers of all the triangles surrounding X_i as shown in Fig. 1. These mass centers will be denoted $(N_i^1, N_i^2, \ldots, N_i^{\Lambda})$, where $\Lambda = \Lambda(i)$ is the number of triangles surrounding X_i, and by convention $N_i^{\Lambda+1} = N_i^1$. At this level, we would like to point out that the actual implementation of the scheme does not require us to store the points N_i^α, but only the vertices for each triangle, the label of the two triangles on both sides of each edge of each triangle, and the label of the two extremities of the edge.

Finally, we set (see Fig. 1)

$$\begin{aligned} |C_i| &= \operatorname{area}(C_i), \\ E_i^{\alpha+1/2} &= (N_i^\alpha, N_i^{\alpha+1}), \\ |E_i^{\alpha+1/2}| &= |N_i^{\alpha+1} - N_i^\alpha|, \end{aligned} \tag{5}$$

and $n_i^{\alpha+1/2}$ (but we will skip the dependence upon i, except if necessary) denotes the outer unit normal to the edge $E_i^{\alpha+1/2}$ joining two consecutive vertices $(N_i^\alpha, N_i^{\alpha+1})$ of the cell C_i.

2.2. Finite Volume Scheme

We are now in a position to describe our finite volume scheme for (1),

$$|C_i|\,(U_i^{n+1} - U_i^n) + \Delta t \sum_{\alpha=1}^{\Lambda(i)} |E_i^{\alpha+1/2}|\,\phi_i^{\alpha+1/2} = 0. \tag{6}$$

The principle of finite volumes is that in this formula, U_i^n represents the *average of* $U(t, x)$ at time $t = n\,\Delta t$ (the time

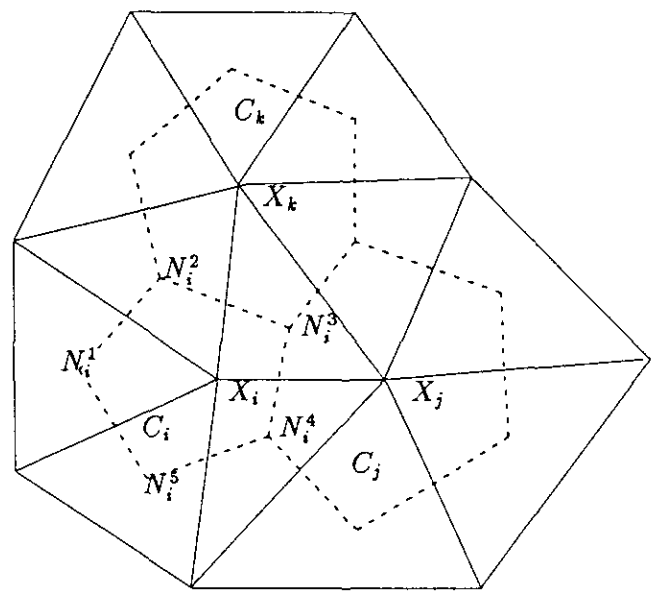

FIG. 1. The control volume used in the finite volume algorithm. Based on a given triangulation X_i, the cell C_i is delimited by the polygon with vertices N_i^α, the mass centers of the corresponding triangles.

step) in the cell C_i. This will be fundamental for our limitation step. The exact flux, deduced from (1) by Green's formula,

$$\frac{1}{|E^{\alpha+1/2}|}\int_{E^{\alpha+1/2}} F(U(t_n, x))\cdot n^{\alpha+1/2}\,dx, \tag{7}$$

is replaced, for second order accuracy, by a simple interpolation

$$\phi_i^{\alpha+1/2} = \tfrac{1}{2}[F(n_i^{\alpha+1/2}, U_i^{\alpha}, U_{j(\alpha)}^{\alpha}) + F(n_i^{\alpha+1/2}, U_i^{\alpha+1}, U_{j(\alpha+1)}^{\alpha+1})], \tag{8}$$

where U_i^{α} represents a second-order accurate interpolation of U at the point N_i^{α}, knowing the values U_i^n. This interpolated value has, however, to be limited within the cell C_i as explained in the next section, and $U_{j(\alpha)}^{\alpha}$ is the same interpolated value at N_i^{α} but limited in the cell $C_j(\alpha)$ neighboring C_i along the edge E_i^{α}. Finally, $F(n, U, V)$ is the normal flux computed by an upwind solver F which should satisfy as usual $F(n, U, U) = F(U)\cdot n$. In Section III, we will describe the kinetic solver and its properties.

In the next section we will describe more precisely the interpolation and limitations in cell algorithms for the dual-type grid. Let us, however, point out that the full algorithm could be performed as well on a rectangular grid. In this case, we have observed, on numerical tests, better results using two "Riemann problems" on each edge, as in (8), rather than one in the middle of the edges. Of course, the drawback of our procedure, on rectangular or triangles based dual grids, is that these two "Riemann problems" could be too expensive. This is one more motivation for using a cheap approximate Riemann solver as the kinetic one. Also we have limited our description to the first order in time algorithm. But second-order accuracy can be achieved as usual using a Runge–Kutta discretization of the underlying ODE (see Osher and Shu [12]), while keeping the nonnegativity properties of the complete algorithm (see Khobalatte and Perthame [11]).

3. INTERPOLATION AND LIMITATION ALGORITHMS

We now describe how we can replace the usual gradient reconstruction by an interpolation + in-cell-limitation algorithm. This gives the values U_i^{α} needed to complete the description of the finite volume algorithm (6), (8). We also prove that this procedure gives second-order accurate values for U_i^{α} and nonnegative values of the density and pressure.

3.1. Interpolation

Let us fix some vertex N_i^{α} of a cell C_i. N_i^{α} is the center of mass of three nodes, say X_i, X_j, X_k of the triangulation, to which are associated three dual cells C_i, C_j, C_k. This makes the interpolation in principle easy (take $\hat{U}^{\alpha} = \frac{1}{3}(U_i^n + U_j^n + U_k^n)$) and motivates us to use the dual grid rather than the triangles directly as control volumes; then the interpolation would be a problem.

There are, however, two difficulties. First the interpolation, as well as gradient reconstruction, should not be performed on the conservative variables U_i^n but on characteristic variables. For gas dynamics, it seems to be enough, and simpler, to work with

$$V_i = (\rho_i^n, (u_1)_i^n, (u_2)_i^n, T_i^n). \tag{9}$$

There is no objection to performing the complete algorithm on the characteristic variables. However, it would be much more expensive because each interpolation should be performed in the local characteristic variables of C_i; they depend upon i.

The second difficulty is that the values U_i^n are the averages of U over the cells C_i. Thus, for U linear which is enough for second-order accuracy, U_i^n are the values of U at the *center of mass* of the cell C_i which, in general, do not coincide with X_i. This leads us to introduce further notations and assumptions:

$$x_i \text{ denotes the center of mass of the cell } C_i, \tag{10}$$

we assume that, as well as X_i, x_i allows us to decompose the cell C_i as the disjoint union of subcells s_i^{α} obtained in joining x_i to the centers of the edges $E_i^{\alpha-1/2}$ and $E_i^{\alpha+1/2}$ (see Fig. 2). (11)

(10) is needed for second-order accuracy and (11) will be needed for our nonnegativity analysis. Whenever (11) is not realized we will prefer to lose accuracy by taking x_i, not the

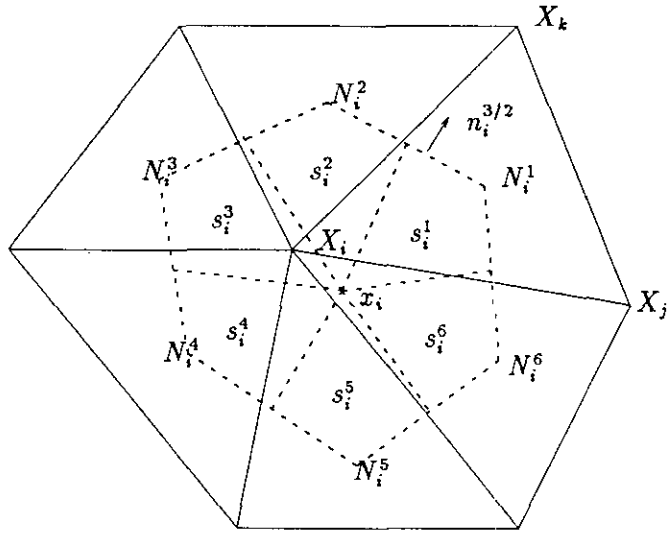

FIG. 2. Subcells s_i^{α} covering the cell C_i associated to the node X_i of the triangulation; x_i is the center of mass of C_i.

center of mass as required, but the closest possible to the center of mass on the interval joining it to X_i, which satisfies (11).

Then, the three point interpolation is performed from (V_i^n, V_j^n, V_k^n) with the weights giving N^α as a combination of (x_i, x_j, x_k). This gives a value $\hat{V}^\alpha$ for $(\hat{\rho}^\alpha, \hat{u}_1^\alpha, \hat{u}_2^\alpha, \hat{T}^\alpha)$ which is common to the three cells C_i, C_j, C_k. Since this interpolation rule is second-order accurate, these values of $\hat{V}^\alpha$ (or more precisely the corresponding conservative quantities $\hat{U}^\alpha$) would give obviously a second-order accurate, but centered, scheme in (6), (8).

Although we do not prove it, it has to be noted that assumption (11) implies that N^α still belongs to the triangle (x_i, x_j, x_k), as well as to the triangle (X_i, X_j, X_k). The barycentric coordinates of N^α with respect to (x_i, x_j, x_k) are thus nonnegative, and our interpolation therefore gives nonnegative values of $\hat{\rho}^\alpha$ and $\hat{T}^\alpha$ in $\hat{V}^\alpha$. In practice, these barycentric coordinates are stored for each triangle once and for all at the beginning of the computation; they only depend on the grid but do not change with time iterations.

3.2. In-Cell-Limitation by Conservation

At this level, we dispose of second-order accurate values $\hat{V}^\alpha$ at the vertices N_i^α with nonnegative densities and pressures. In this subsection, we determine new values V^α using a limitation procedure within the cell C_i, which meets three requirements,

(i) the limited values $V_i^\alpha = (\rho_i^\alpha, (u_1)_i^\alpha, (u_2)_i^\alpha, T_i^\alpha)$ are still second-order accurate,

(ii) the limited densities and pressures $\rho_i^\alpha, T_i^\alpha$ are still nonnegative,

(iii) the global conservation holds in the cell C_i, i.e.,

$$|C_i|\, U_i^n = \sum_{\alpha=1}^{A(i)} |s_i^\alpha|\, U_i^\alpha, \tag{12}$$

where $|s_i^\alpha|$ is the area of the subcell s_i^α in (11) and U_i^α are the limited conservative variables deduced from V_i^α. This means that we have really in mind that the representation of U^n is piecewise constant in the subcells s_i^α. This is not a second-order approximation of $U^n(x)$. But only the vertices N^α are important in (8) and there it is second-order accurate. We base this limitation on conservation.

3.2.1. *Conservation of Mass*

Truncate together among the interpolated values $\hat{\rho}^\alpha$, all those that are either larger or smaller than the known average ρ_i in the cell C_i so as to impose conservation. This means, set

$$\rho_i^\alpha = \rho_i^n + \beta_+ (\hat{\rho}^\alpha - \rho_i^n)_+ - \beta_- (\hat{\rho}^\alpha - \rho_i^n)_-, \tag{13}$$

where $0 \leqslant \beta_-, \beta_+ \leqslant 1$ are chosen with either $\beta_+ = 1$ and $\beta_- \leqslant 1$ or $\beta_- = 1$ and $\beta_+ \leqslant 1$ by the relation

$$\sum_{\alpha=1}^{A(i)} |s_i^\alpha|\, \rho_i^\alpha = \sum_{\alpha=1}^{A(i)} |s_i^\alpha|\, \rho_i^n = |C_i|\, \rho_i^n. \tag{14}$$

This is achieved by the only possible choice

$$\beta_\pm = \min\left(1, \sum_\alpha |s_i^\alpha|\, (\hat{\rho}^\alpha - \rho_i^n)_\mp \Big/ \sum_\alpha |s_i^\alpha|\, (\hat{\rho}^\alpha - \rho_i^n)_\pm\right), \tag{15}$$

and we have used the notation $x_+ = \max(0, x)$, $x_- = \max(0, -x)$.

Note that, in one dimension, α takes only two values and this is exactly the min-mod limitation.

3.2.2. *Conservation of Momentum*

For $u = u_1$ or u_2 (and dropping the indices i and n), we set, similarly,

$$u^\alpha = u + \beta_+ (\hat{u}^\alpha - u)_+ - \beta_- (\hat{u}^\alpha - u)_-, \tag{16}$$

with

$$\beta_\pm = \min\left(1, \sum_\alpha |s^\alpha|\, \rho^\alpha (\hat{u}^\alpha - u)_\mp \Big/ \sum_\alpha |s^\alpha|\, \rho^\alpha (\hat{u}^\alpha - u)_\pm\right), \tag{17}$$

where ρ^α is previously computed. And again we obtain the conservation of momentum

$$\sum_\alpha |s^\alpha|\, \rho^\alpha u^\alpha = \sum_\alpha |s^\alpha|\, \rho u = |C|\, \rho u. \tag{18}$$

3.2.3. *Conservation of Energy*

Using $\rho^\alpha, u_1^\alpha, u_2^\alpha$ computed before, we set

$$T^\alpha = T - (\gamma - 1)[(u_1^\alpha - u_1)^2 + (u_2^\alpha - u_2)^2]/2 + \beta_+ (\hat{T}^\alpha - T)_+ + \beta_- (\hat{T}^\alpha - T), \tag{19}$$

where

$$\beta_\pm = \min\left(1, \sum_\alpha |s^\alpha|\, \rho^\alpha (\hat{T}^\alpha - T)_\mp \Big/ \sum_\alpha |s^\alpha|\, \rho^\alpha (\hat{T}^\alpha - T)_\pm\right). \tag{20}$$

And conservation of energy now means

$$\sum_\alpha |s^\alpha|\, \rho^\alpha \left(\frac{(u_1^\alpha)^2}{2} + \frac{(u_2^\alpha)^2}{2} + \frac{T^\alpha}{\gamma - 1}\right) = |C|\, E, \tag{21}$$

as proved in

PROPOSITION 1. *The limitation* (13), (15), (16), (17), (19), (20) *satisfies the conservation laws* (14), (18), (21).

Proof of Proposition 1. We only prove the last conservation because they are all obtained by the same argument. Using the conservation of mass and momentum we have

$$\begin{aligned}\sum_\alpha s^\alpha \rho^\alpha (u_1^{\alpha 2} + u_2^{\alpha 2}) &= \sum_\alpha s^\alpha \rho^\alpha ((u_1^\alpha - u_1)^2 + (u_2^\alpha + u_2)^2 \\ &\quad - u_1^2 - u_2^2 + 2u_1 u_1^\alpha + 2u_2 u_2^\alpha) \\ &= \sum_\alpha s^\alpha \rho^\alpha ((u_1^\alpha - u_1)^2 + (u_2^\alpha - u_2)^2) \\ &\quad + \sum_\alpha s^\alpha \rho (u_1^2 + u_2^2).\end{aligned}$$

Therefore

$$\begin{aligned}\sum_\alpha s^\alpha \rho^\alpha [(u_1^{\alpha 2} + u_2^{\alpha 2})(\gamma - 1)/2 + T^\alpha] &= \sum_\alpha s^\alpha \rho^\alpha (u_1^2 + u_2^2)(\gamma - 1)/2 + \sum_\alpha s^\alpha \rho^\alpha T \\ &= \sum_\alpha s^\alpha \rho^\alpha [(u_1^2 + u_2^2)(\gamma - 1)/2 + T] \\ &= |C|\, E(\gamma - 1).\end{aligned}$$

This proves the conservation of energy. ∎

Remark. The idea that the temperature T has to be corrected by the value $(\gamma - 1)\,|u|^2/2$ for positivity was introduced in [13] in 1D.

We now prove that this reconstruction gives nonnegative values of ρ^α, T^α.

PROPOSITION 2. *If the interpolated values satisfy* $\hat\rho^\alpha \geqslant 0$, $\hat T^\alpha \geqslant 0$, *and*

$$\begin{aligned}(\gamma - 1)(\hat u_1^\alpha - u_1)^2 &\leqslant T, \\ (\gamma - 1)(\hat u_2^\alpha - u_2)^2 &\leqslant T\end{aligned} \tag{22}$$

for all $1 \leqslant \alpha \leqslant \alpha_M$, *then the corrected values satisfy* $\rho^\alpha \geqslant 0$, $T^\alpha \geqslant 0$.

Proof of Proposition 2. Given α, the limitations (13), (16) yield

$$\begin{aligned}&|u_1^\alpha - u_1| \leqslant |\hat u_1^\alpha - u_1|, \\ &|u_2^\alpha - u_2| \leqslant |\hat u^\alpha - u_2|, \\ &\rho^\alpha \in [\rho, \hat\rho^\alpha].\end{aligned}$$

Since $\hat\rho^\alpha$ and ρ are nonnegative this gives $\rho^\alpha \geqslant 0$. And (19) immediately gives $T^\alpha \geqslant 0$. ∎

We conclude this section by proving that this limitation preserves the second-order accuracy of the interpolation.

THEOREM 3. *We assume* (10), (11). *If the interpolated values* $\hat V^\alpha$ *are second-order accurate approximations of exact values* $V(N^\alpha)$, *then the corrected values are also second-order accurate approximations of* $V(N^\alpha)$.

COROLLARY 4. *We assume* (10), (11), *then the fluxes in* (8) *are second-order approximations of the exact fluxes* (7).

Corollary 4 is an immediate consequence of Theorem 3 since in (6) the integration on the edges is performed with second-order accuracy. As usual for finite volumes on irregular meshes, it does not mean that the full scheme is second-order accurate. This only holds for grids with special symmetries. On numerical results, we, however, observe an obvious improvement compared to the scheme with first-order fluxes (which again does not mean first-order truncating error).

Proof of Theorem 3. Let us concentrate on the density variable, for instance (for the other variables, the proof goes the same way). Our limitation algorithm is Lipschitz continuous because it contains only Lipschitz continuous algebraic operations except if $\sum_\alpha (\rho^\alpha - \rho)_+ = 0$ (or $(\ldots)_-$) which means that no limitation is performed. Therefore it is enough to check that if $\rho(x)$ is a linear function and $\hat\rho^\alpha$ are the exact values $\rho(N^\alpha)$, then the limitation step gives indeed $\hat\rho^\alpha = \rho(N^\alpha)$ (in other words it is exact for linear functions). In that case we can write

$$\rho(x) = \rho(x_i) + D\rho \cdot (x - x_i), \qquad \rho_i = \rho(x_i); \tag{23}$$

thus we obtain

$$\sum_{\alpha=1}^{A(i)} |s_i^\alpha|\, (\hat\rho^\alpha - \rho_i) = D\rho \cdot \sum_{\alpha=1}^{A(i)} |s_i^\alpha|\, (N_i^\alpha - x_i) = 0, \tag{24}$$

because we have for the dual grid of Section I

$$\sum_{\alpha=1}^{A(i)} |s_i^\alpha|\, (N_i^\alpha - x_i) = 0, \tag{25}$$

as will be proved in Lemma 5 below. This means that

$$\sum_\alpha |s_i^\alpha|\, (\hat\rho^\alpha - \rho_i)_+ = \sum_\alpha |s_i^\alpha|\, (\hat\rho^\alpha - \rho_i)_-. \tag{26}$$

and thus $\beta_+ = \beta_- = 1$, which proves that no limiting arises for linear functions. And the proof of Theorem 3 will be completed by

LEMMA 5. *Under assumptions* (10) *and* (11) *the triangle-based dual grid presented in Section* 1 *satisfies* (25).

Proof of Lemma 5. Let us introduce the mass centers y^α of the triangles $K^\alpha = (x_i, N_i^\alpha, N_i^{\alpha+1})$ which are included in

the cell C_i by assumption (11). For a triangle the mass center is given by the formula

$$y^\alpha = (x_i + N_i^\alpha + N_i^{\alpha+1})/3, \qquad |K^\alpha|\ y^\alpha = \int_{K^\alpha} x\,dx. \quad (27)$$

Since, again by (11), C_i is the disjoint union of the K^α, we find that

$$\begin{aligned} |C_i|\ x_i &= \int_{C_i} x\,dx = \sum_\alpha |K^\alpha|\ y^\alpha \\ &= \sum_\alpha |K^\alpha|\ (N_i^\alpha + N_i^{\alpha+1})/3 + |C_i|\ x_i/3, \end{aligned}$$

and thus

$$\begin{aligned} |C_i|\ x_i &= \sum_\alpha |K^\alpha|\ (N_i^\alpha + N_i^{\alpha+1})/2 \\ &= \sum_\alpha |s_i^\alpha|\ N_i^\alpha, \end{aligned}$$

because $2\,|s_i^\alpha| = |K^\alpha| + |K^{\alpha-1}|$. ∎

4. BOLTZMANN SOLVER FOR GAS DYNAMICS AND NONNEGATIVITY

The purpose of this section is to show how a kinetic solver can be implemented together with the interpolation procedure of Section II in order to keep the nonnegativity property of the density and pressure obtained in Proposition 2. This leads us to derive a rigorous CFL condition. In that sense the nonnegativity requirement is a stability condition. Also it implies, together with the conservation of mass and energy, an L^1 bound on ρ, ρT, and ρu (since by Cauchy–Schwarz inequality) $(\int |\rho u|)^2 \leqslant (\int \rho)(\int \rho u^2))$ and thus it gives a nonlinear weak stability result in the sense of a priori bounds on the solution.

For a rectangular mesh, the kinetic solver allows to take into account the corners effects which are important for first order schemes (see [13]). This is no longer possible for an unstructured grid and the numerical tests we have performed on a rectangular grid show that, after our second-order reconstruction, these corner effects play no role.

In the first subsection below we describe the "simplified" Boltzmann solver and then we prove, in Subsection 2, the nonnegativity property for a classical CFL condition. Of course, any other solver could be used if this nonnegativity property is not required.

4.1. Description of the Riemann Solver

We now describe the solver, which means the approximate flux $F(n, U, W)$ in the scheme (8). We are going to use a Boltzmann solver (see Harten, Lax, and Van Leer [10] for the terminology), which are flux splittings of Van Leer type ([18]):

$$F(n, U, W) = F^+(n, U) + F^-(n, W), \qquad (28)$$

with

$$F^+(n, U) = \rho \int_{\{\xi\cdot n \geqslant 0\}} \xi\cdot n \begin{pmatrix} 1 \\ \xi \\ \dfrac{|\xi|^2}{2} + \lambda T \end{pmatrix} \chi\left(\frac{\xi - u}{\sqrt{T}}\right)\frac{d\xi}{T}, \quad (29)$$

and F^- is obtained integrating over the set $\{\xi\cdot n \leqslant 0\}$. Here $\xi \in \mathbb{R}^2$ and λ is related to γ in the pressure law (4) by

$$\lambda = \frac{2-\gamma}{2(\gamma-1)}. \qquad (30)$$

The motivation for introducing these numerical fluxes is that they correspond to a kinetic description of the gas. Given the initial data

$$\begin{aligned} f_0(x, \xi) &= \frac{\rho_0(x)}{T_0(x)}\,\chi\left(\frac{\xi - u_0(x)}{\sqrt{T_0(x)}}\right), \\ g_0(x, \xi) &= \lambda T_0(x)\, f_0(x, \xi), \end{aligned} \qquad (31)$$

the free transport equations

$$\partial_t f + v\cdot\nabla_x f = 0, \qquad \partial_t g + v\cdot\nabla_x g = 0, \qquad (32)$$

are related to the gas dynamics equation.

Indeed, the conservative variables and the fluxes in (1) can be represented by

$$U_0(x) = \int_{\xi\in\mathbb{R}^2} \left[\begin{pmatrix} 1 \\ \xi \\ |\xi|^2/2 \end{pmatrix} f_0(x, \xi) + \begin{pmatrix} 0 \\ 0 \\ 1 \end{pmatrix} g_0(x, \xi) \right] d\xi, \quad (33)$$

$$F(U_0)\cdot n = F^+(n, U_0) + F^-(n, U_0) \quad \text{for every } n \in \mathbb{R}^2, \quad (34)$$

as soon as χ satisfies

$$\begin{aligned} &\int_{\mathbb{R}^2} (1, w_k, w_h w_l)\,\chi(w)\,dw \\ &\qquad = (1, 0, \delta_{hl}), \qquad 1 \leqslant h, l \leqslant 2. \end{aligned} \qquad (35)$$

Note that (34) is nothing but the consistancy of the numerical flux (28), $F(n, U, U) = F(U)\cdot n$, and that (33), (34) mean that, during a small time step Δt, the appropriate combinations of the integrals of f and g, as in (33), are first-order (in Δt) approximations of the gas dynamics equations (1)–(4).

Several choices of χ are possible that meet the requirement (35). In [4, 14], the choice of "maxwellians" relevant for Navier–Stokes flows, is used,

$$\chi(w)=\frac{1}{2\pi}e^{-|w|^2/2}. \tag{36}$$

Another multidimensional choice of χ is ($\prod$ denotes the indicator function)

$$\chi(w)=\frac{1}{4\pi}\prod(|w|\leqslant 2). \tag{37}$$

Among all the possible choices a more complicated χ is proposed in Khobalatte and Perthame [11] which satisfies the maximum principle on the specific entropy.

But in order to obtain a cheaper solver, we take in practice

$$\chi(n,w)=\tfrac{1}{12}\prod(|w_1|\leqslant\sqrt{3})\qquad\prod(|w_2|\leqslant\sqrt{3}), \tag{38}$$

where w_1, w_2 are the coordinates such that $n=(1,0)$. Then, the formula (29) is particularly simple to integrate. Note that with the choice (38), the flux (as well as χ) depends explicitly on the normal. Thus, it is not guenuinely multidimensional, while the fluxes deduced from (36) or (37) are, in the sense that they satisfy

$$F(R\cdot n,\mathscr{R}\cdot U,\mathscr{R}W)=\mathscr{R}\cdot F(n,U,W)$$

for all unitary transforms R, and with $\mathscr{R}\cdot(\rho,u,T)=(\rho,R\cdot u,T)$.

4.2. Stability Analysis

We now prove the nonnegativity of the densities and pressures computed with the scheme (6), (8), together with the kinetic flux (29), (37).

THEOREM 6. *Consider the scheme* (6), (8) *with fluxes defined by* (28)–(30) *and* (38) *and with a conservative prediction of* U_i^α *satisfying* $\rho_i^\alpha\geqslant 0$, $T_i^\alpha\geqslant 0$. *It gives* $\rho_i^{n+1}\geqslant 0$, $T_i^{n+1}\geqslant 0$ *under the CFL condition*

$$(|u_i^\alpha|+\sqrt{3T_i^\alpha})\,\Delta t\,|E^{\alpha\pm 1/2}|\leqslant 2\,|C_i|,\qquad\forall i,\alpha, \tag{40}$$

with the notations (5).

Proof of Theorem 6. We introduce the kinetic representation of the gas at time $n\,\Delta t$ in the subcell s_i^α,

$$f_i^{\alpha,\pm}(\xi)=\frac{\rho_i^\alpha}{T_i^\alpha}\chi\left(n_i^{\alpha\pm 1/2},\frac{\xi-u_i^\alpha}{\sqrt{T_i^\alpha}}\right), \tag{41}$$

$$g_i^{\alpha,\pm}(\xi)=\lambda\rho_i^\alpha\chi\left(n_i^{\alpha\pm 1/2},\frac{\xi-u_i^\alpha}{\sqrt{T_i^\alpha}}\right), \tag{42}$$

These quantities are related to U_i^α by

$$\int_{\mathbb{R}^2}\left[\begin{pmatrix}1\\ \xi\\ |\xi|^2/2\end{pmatrix}f_i^{\alpha,\pm}(\xi)+\begin{pmatrix}0\\ 0\\ 1\end{pmatrix}g_i^{\alpha,\pm}(\xi)\right]d\xi=U_i^\alpha, \tag{43}$$

which is a straightforward consequence of (33). Then, we define the kinetic representation at time $(n+1)\,\Delta t$ by means of a finite volume approximation of the transport equation (32),

$$\begin{aligned}|C_i|\,f_i^{n+1}(\xi)=&\sum_{\alpha=1}^{A(i)}\frac{|s_i^\alpha|}{2}(f_i^{\alpha,+}(\xi)+f_i^{\alpha,-}(\xi))\\&+\frac{\Delta t}{2}\sum_{\alpha=1}^{A(i)}|E_i^{\alpha+1/2}|\,[(\xi\cdot n_i^{\alpha+1/2})_-\\&\times(f_j^{\beta,+}(\xi)+f_j^{\beta,-}(\xi))\\&-(\xi\cdot n_i^{\alpha+1/2})_+(f_i^{\alpha,+}(\xi)\\&+f_i^{\alpha+1,-}(\xi))],\end{aligned} \tag{44}$$

and the same formula, replacing f by g, allows us to define $g_i^{n+1}(\xi)$. In (13), $j=j(i,\alpha+\frac{1}{2})$ and β stand for the labels of the subcells neighboring C_i along the edge $E^{\alpha+1/2}$. In fact (45) amounts to writing the scheme (6), (8) with fluxes given by (28), (29), (38). Indeed, if we define

$$\begin{aligned}U_i^{n+1}&=\begin{pmatrix}\rho_i^{n+1}\\ (\rho u)_i^{n+1}\\ E_i^{n+1}\end{pmatrix}\\&=\int_{\mathbb{R}^2}\left[\begin{pmatrix}1\\ \xi\\ |\xi|^2/2\end{pmatrix}f_i^{n+1}(\xi)+\begin{pmatrix}0\\ 0\\ 1\end{pmatrix}g_i^{n+1}(\xi)\right]d\xi,\end{aligned} \tag{45}$$

then, the integration $d\xi$ of (44) (with the weights 1, ξ, $|\xi|^2/2$) combined with the integration of the equation for g^{n+1}, as in (33), yields exactly

$$|C_i|\,U_i^{n+1}=|C_i|\,U_i^n+\Delta t\sum_{\alpha=1}^{A(i)}|E_i^{\alpha+1/2}|\,\phi_i^{\alpha+1/2}=0,$$

with the right fluxes $\phi_i^{\alpha+1/2}$. This just follows from (43) and (recall (14), (18), (21))

$$\sum_\alpha|s_i^\alpha|\,U_i^\alpha=|C_i|\,U_i^n.$$

Now, thanks to (44), in order to prove the nonnegativity of ρ_i^{n+1}, T_i^{n+1}, it remains to check that f_i^{n+1} and g_i^{n+1} are nonnegative which follows from (44) as soon as

$$\frac{1}{2}|s_i^\alpha|\geqslant\frac{\Delta t}{2}|E_i^{\alpha\pm 1/2}|\,(\xi\cdot n^{\alpha+1/2}), \tag{46}$$

for ξ in the support of χ. Such ξ satisfy, see (38),

$$|\xi \cdot n| \leqslant |u_i^z| + \sqrt{3T_i^z},$$

and thus (46) is only the announced CFL condition, and Theorem 6 is proved. ▮

5. NUMERICAL RESULTS

We now present several numerical tests performed with the above method processed on various triangle-based dual grids (we always present the primal triangulation together with the numerical results). These tests were chosen to show both the accuracy and the stability of the method. Except for the global flow around an ellipse, these tests are all standard and our results are comparable with the existing literature.

5.1. 1D Problems Computed on a 2D Triangular Grid

These problems have the advantage of being very standard and the results are easy to analyze. We have used a random triangulation of a rectangle and we have computed planar waves associated to two problems. Note that the number of triangles we have amounts to 140 grid points in the horizontal direction. Figure 3 shows the results

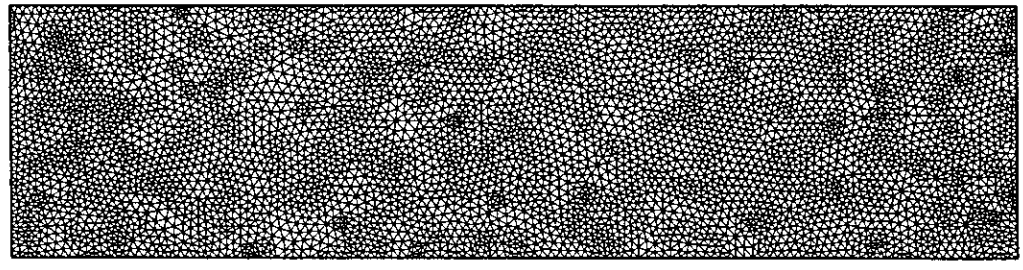

(a)

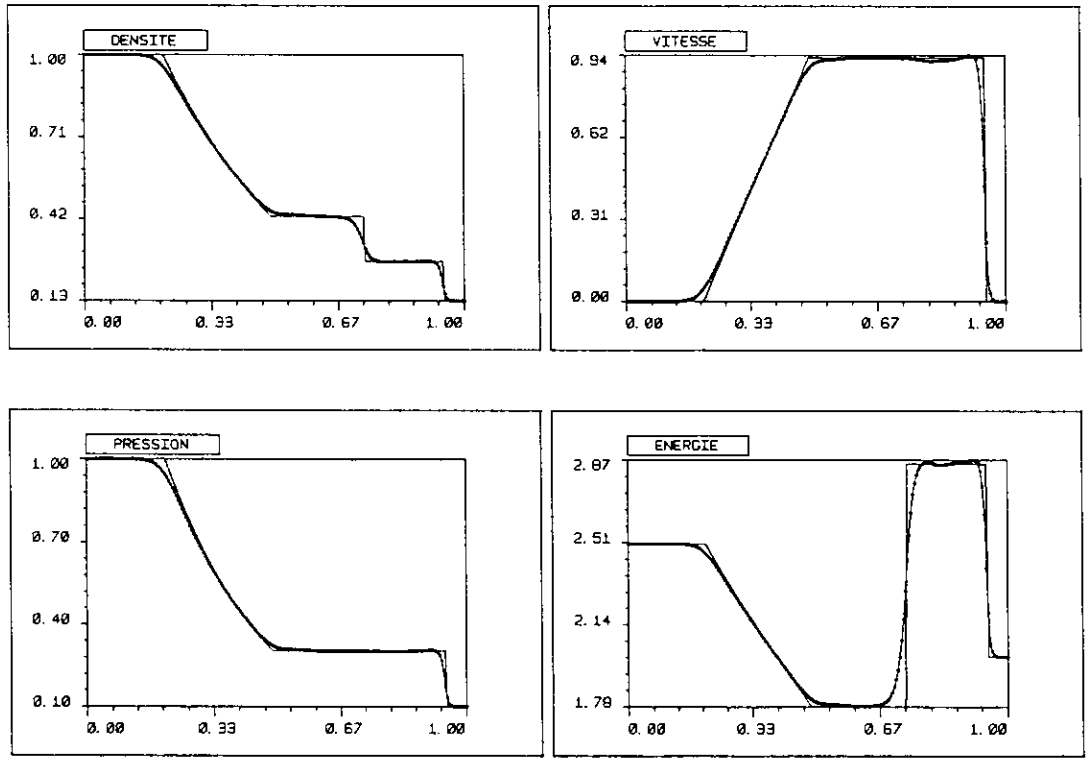

(b)

FIG. 3. (a) Random triangulation for the 1D problems, 4805 nodes, 9296 triangles. This amounts to 140 grid points in the horizontal direction. (b) Sod shock tube. Comparison of the exact solution and the computed solution with the second-order scheme (in time and space).

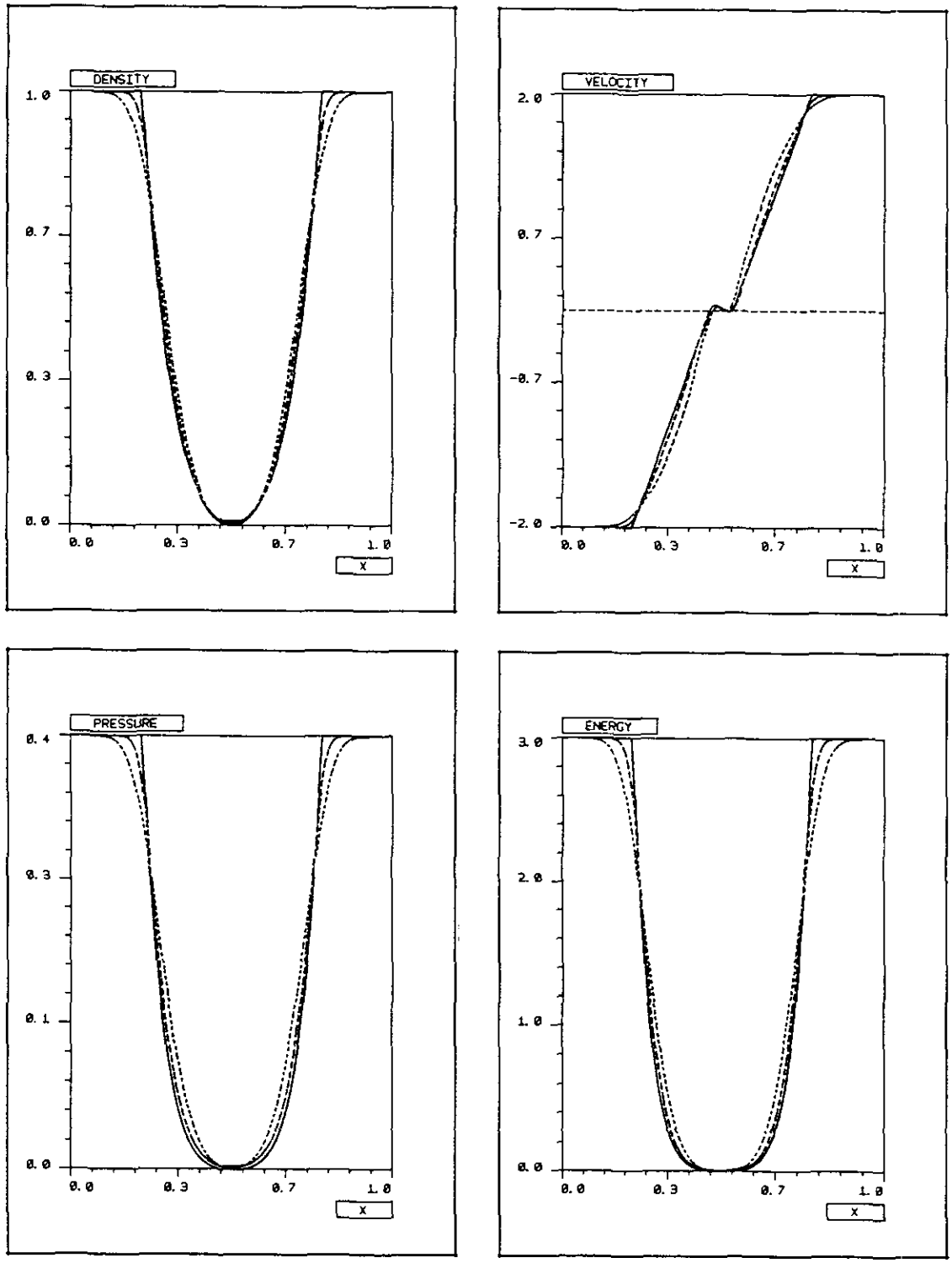

FIG. 4. Riemann problem 1-2-0-3 of [7]. Comparison of the exact solution and the computed solution with the first- and second-order schemes (in time and space).

obtained for Sod's shock tube. We compare the exact solution with the results of our schemes. The second-order results are very superior to those obtained with the 1D first-order scheme, even though they do not reach exactly the accuracy of 1D second-order schemes. With this grid size, we did not note any improvement when using a regular grid deduced from a rectangular mesh.

We have chosen another 1D test problem proposed recently in [7] for its difficulty because the density and pressure vanish. It is a Riemann problem called 1-2-0-3 in [7]. As predicted by the theory, our second-order 2D algorithm did not generate any negative density or pressure. The results are presented in Fig. 4; we compare the exact solution to the results obtained by the first-order and second-order schemes. A very neat improvement can be seen although this test is less selective for accuracy than Sod's tube.

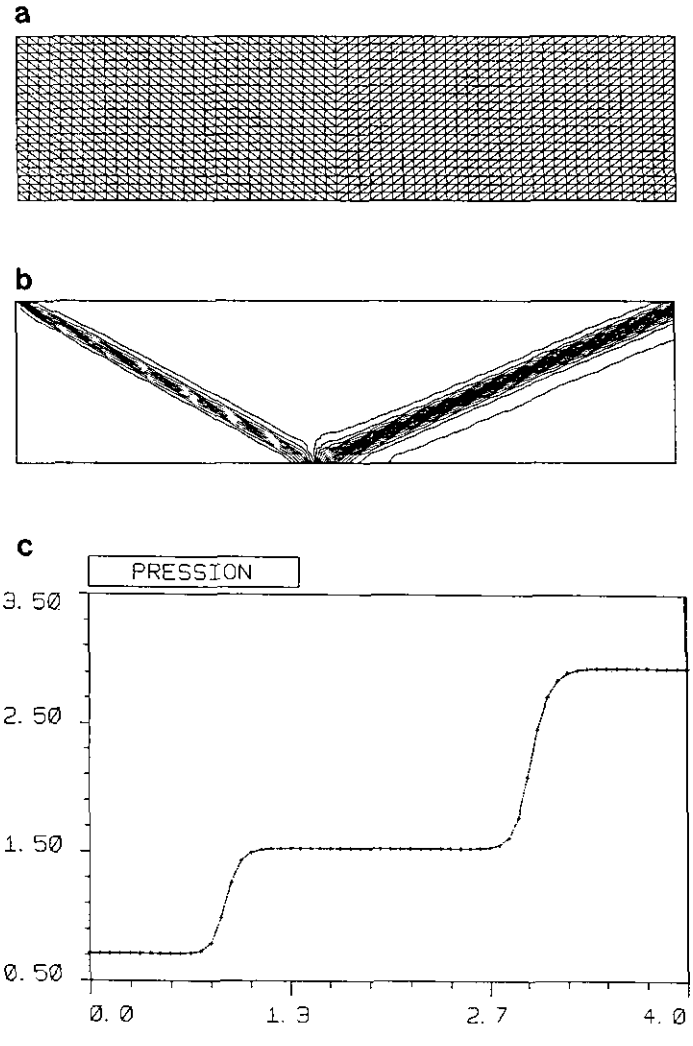

FIG. 5. (a) Regular grid, 1281 nodes, 2400 triangles. (b) Pressure isolines, min = 0.71, max = 2.94, 25 isovalues. (c) Horizontal pressure profile in the middle of the rectangle.

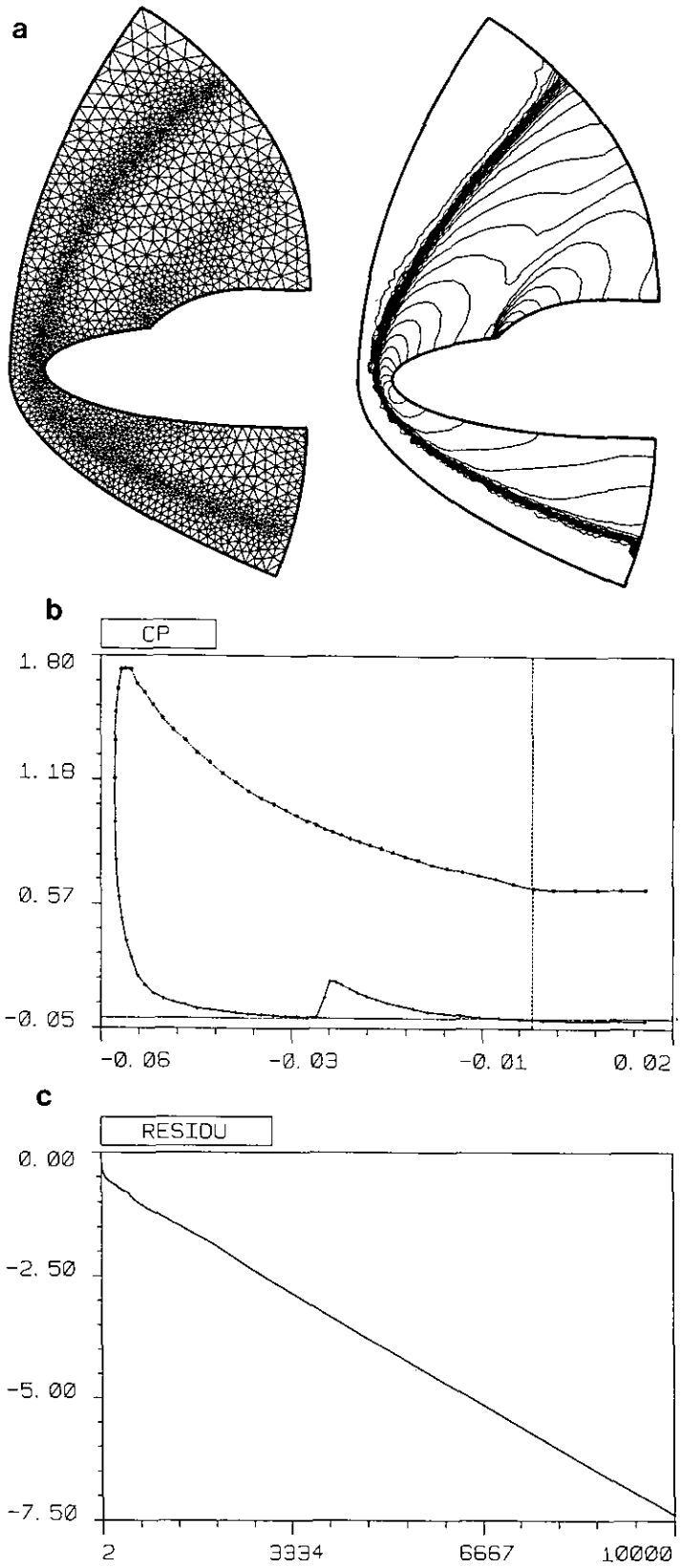

FIG. 6. (a) Triangular grid, 2258 nodes, 4295 elements, and Mach isolines, min = 0.03, max = 8.15. (b) C_p profile along the body. (c) Convergence (in logs) history.

5.2. 2D Problems

The first 2D test we present in Fig. 5 is the reflexion problem. It is very standard and very accurate results can be found in [2]. The constant states between the two shocks are very well computed by our algorithm and very flat (we present here the pressure but similar profiles are obtained on the velocity or density). Also the shocks are rather good (three grid points for the incident shock and five grid points for the reflected shock).

One of the interests of triangular-based grids is the possibility to perform local adaptation of the grid. Our next 2D test problems are chosen to be very difficult from the stability point of view because of hypersonic regimes and locally distorted meshes. The first test is the double ellipse problem and the results are shown in Fig. 6.

It is interesting to note the very good decay of the residue, which shows that the iterations really lead to a stationary solution and confirm that the interpolation limitation procedure is stable. For accuracy, many results for this test are presented in the Hermes Workshop [5] and our results are comparable to the best in [5].

To assert the nonnegativity property, we have chosen a particularly difficult problem: a global flow around an

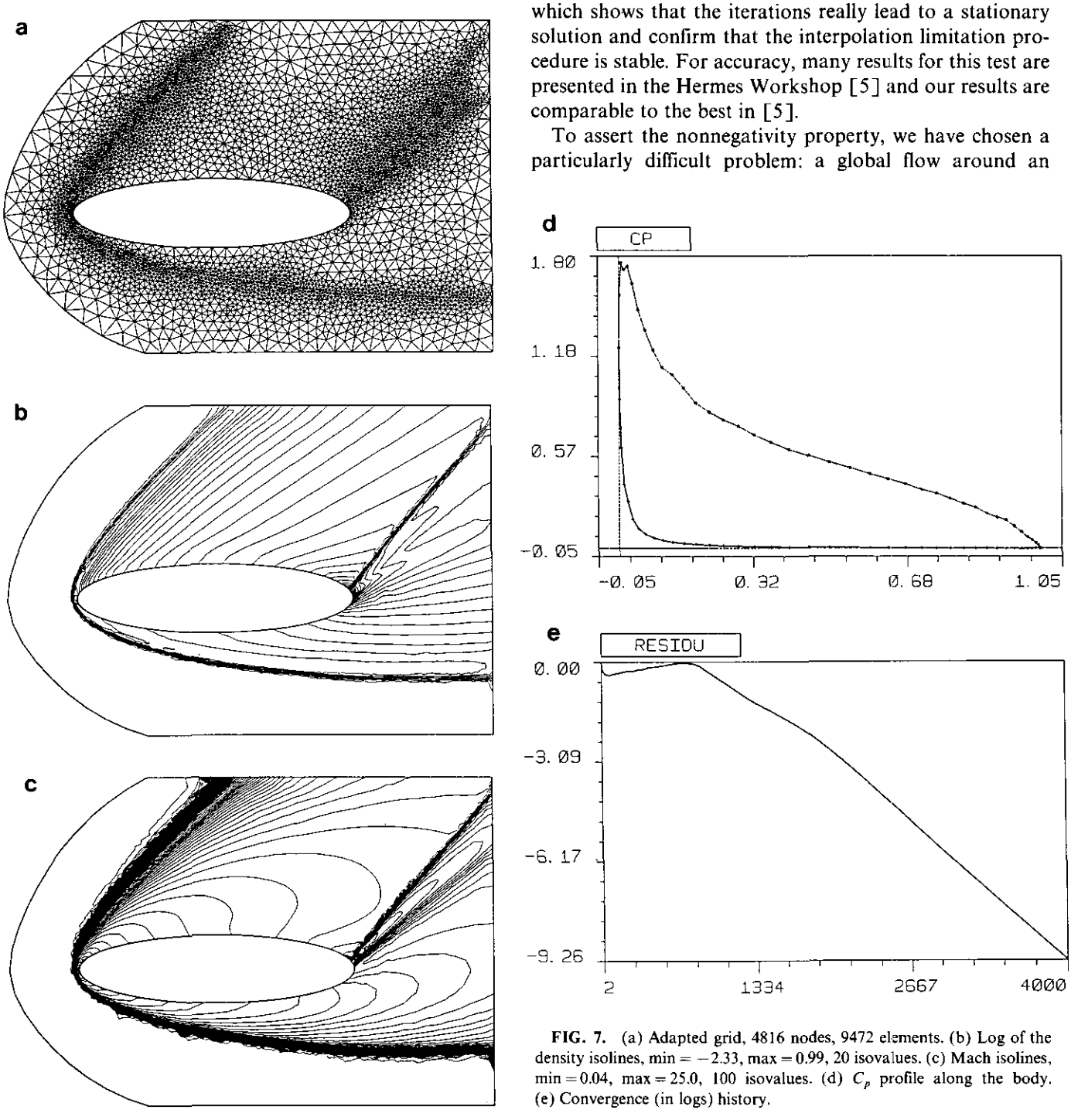

FIG. 7. (a) Adapted grid, 4816 nodes, 9472 elements. (b) Log of the density isolines, min = −2.33, max = 0.99, 20 isovalues. (c) Mach isolines, min = 0.04, max = 25.0, 100 isovalues. (d) C_p profile along the body. (e) Convergence (in logs) history.

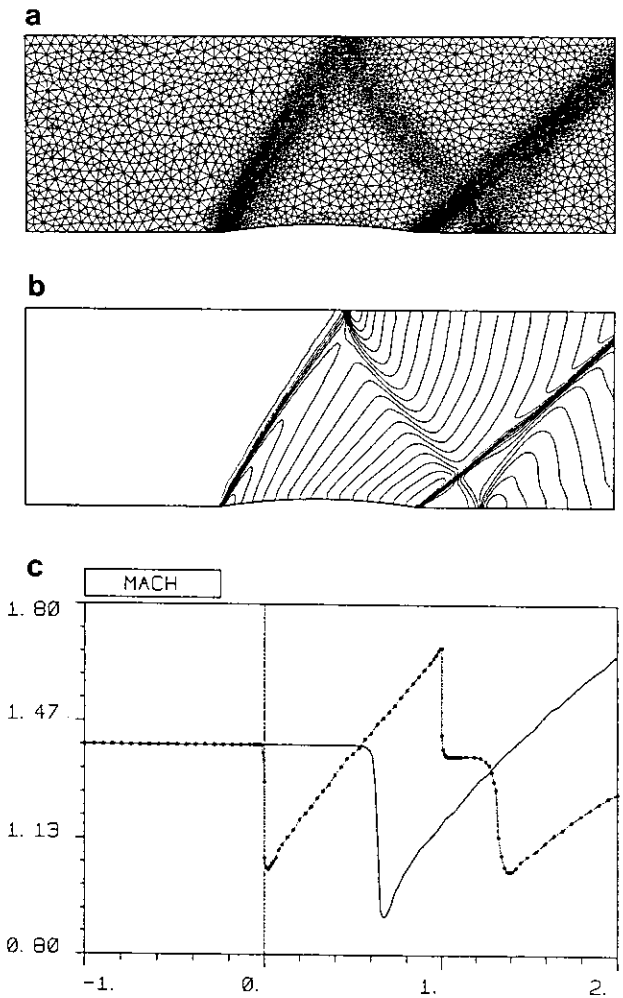

FIG. 8. (a) Adapted grid, 5339 nodes, 10451 elements. (b) Mach isolines, min = 0.91, max = 1.67, $M_\infty = 1.4$, 20 isovalues. (c) Mach profiles at the top and bottom edges of the domain.

ellipse with a Mach number of 25, an incidence of 30°, and $\gamma = 1.2$. Many authors have reported negative pressures behind the body. Our code gave a stationary positive solution, shown in Fig. 7. The same residue decay is observed in Fig. 5.

Finally, to show again that our results are comparable to other second-order schemes, we present in Fig. 8 a Mach 2 channel problem with a circular 4° bump. This test is also classical and recent results can be found in [17], for instance. The shocks are rather well computed but it is noticeable that there are absolutely no oscillations.

REFERENCES

1. F. Angrand, A. Dervieux, V. Boulard, J. Périaux, and G. Vijayasundaram, "Transonic Euler Simulations by Means of Finite Element Explicit Schemes," in *AIAA-83*, 1984.
2. P. Colella, *J. Comput. Phys.* **87**, 171 (1990).
3. F. Coquel and M. S. Liu, "Stable and Low Diffusive Hybrid Upwind Splitting Methods," in *First European Computational Fluid Dynamics Conf., Brussels 1992* and ONERA Preprint No. 113, 1992.
4. S. M. Desphande, NASA Technical Paper No. 2613, 1986 (unpublished).
5. J. A. Desideri, R. Glowinski, and J. Périaux (Eds.), *Hypersonic Flows for Reentry Problems*, Vol. II (Springer-Verlag, New York/Berlin, 1991).
6. L. J. Durlofsky, B. Engquist, and S. Osher, CAM Report 89-33, UCLA, 1989 (unpublished).
7. E. Einfeldt, C. D. Munz, P. L. Roe, and B. Sjögreen, *J. Comput. Phys.* **92**, 273 (1991).
8. L. Fezoui and B. Larrouturou, "On the Equations of Multicomponent Perfect or Real Gas Inviscid Flow, in *Nonlinear hyperbolic problems, Bordeaux, 1988*, p. 69, Lecture Notes in Math., Vol. 1402 (Springer-Verlag, Berlin, 1989).
9. A. Harten, *J. Comput. Phys.* **49**, 357 (1983).
10. A. Harten, P. D. Lax, and B. Van Leer, *SIAM Rev.* **25**, 35 (1983).
11. B. Khobalatte and B. Perthame, INRIA Report No. 1628; *Math. Comput.*, to appear.
12. S. Osher and C. W. Shu, *J. Comput. Phys.* **83**, 32 (1989).
13. B. Perthame, *SIAM J. Numer. Anal.* **29**, No. 1 (1992).
14. D. I. Pullin, *J. Comput. Phys.* **34**, 231 (1980).
15. P. Rostand and B. Stoufflet, "TVD Schemes to Compute Compressible Viscous Flows on Unstructured Meshes, in *Notes on Numerical Fluid Mechanics*, Vol. 24, edited by J. Ballmann and R. Jeltsch (Vieweg, Wiesbaden, 1988), p. 510.
16. R. Sanders and A. Weiser, *J. Comput. Phys.* **101**, 314 (1992).
17. R. Struijs, H. Deconinck, P. De Palma, P. Roe, and K. G. Powell, "Progress on Multidimensional Upwind Euler Solvers for Unstructured Grids," in *AIAA 91-1550.*
18. B. Van Leer, *J. Comput. Phys.* **32**, 101 (1979).
19. B. Van Leer, "Flux Vector Splitting for the Euler Equations," in *8th International Conference on Numerical Methods in Fluid Dynamics*, edited by E. Krause, Lecture Note in Physics, Vol. 170 (Springer-Verlag, Berlin, 1982), p. 507.